Angular dispersion and polarization mixing in GaAs/AlAs superlattices grown along the [012] direction

Z. V. Popović* and M. Cardona
Max-Planck-Institut für Festkörperforschung, D-7000 Stuttgart 80, Federal Republic of Germany

E. Richter and D. Strauch
Institut für Theoretische Physik, Universität Regensburg, D-8400 Regensburg, Federal Republic of Germany

L. Tapfer and K. Ploog
Max-Planck-Institut für Festkörperforschung, D-7000 Stuttgart 80, Federal Republic of Germany
(Received 2 July 1990)

Results of lattice-dynamical calculations of the GaAs/AlAs superlattice grown along the [012] direction are compared with Raman-scattering data. Confined phonon modes and the in-plane (interfacelike) optical modes are clearly observed at frequencies in excellent agreement with theoretical predictions. The confined phonons of the [012]-oriented superlattice have mixed longitudinal and transverse character, as a consequence of the low symmetry of this superlattice (C_2 point group). Special emphasis is placed on the angular dispersion and mixed polarization of superlattice modes.

I. INTRODUCTION

The vibrational properties of GaAs/AlAs superlattices (SL's) grown on GaAs substrates for directions other than [001] were practically unknown until recently.[1-4] Results given in these references indicate that the phonons and their Raman spectra for GaAs/AlAs SL's grown along [012],[1,2] [110],[3] and [111] (Ref. 4) directions differ from those of SL's grown along the [001] direction[5] due to the different crystal symmetries. In the case of GaAs/AlAs SL's grown along the [001] and [111] directions, the confined modes have either purely longitudinal or transverse polarization. In all [0ij] superlattices there is a twofold rotation axis perpendicular to the direction of growth. Consequently the confined modes are either odd or even with respect to rotation about this axis. This property is not true, in general; for example, in the case of [111] superlattices.[4] The GaAs/AlAs SL grown along the [110] direction is particularly interesting as its confined phonons have either transverse (eigenvector parallel to the [1$\bar{1}$0] direction) or mixed longitudinal (parallel to [110]) and transverse (parallel to [001]) polarization.[3] In the case of a [012]-oriented SL, no pure longitudinal or transverse modes exist. The mixed polarization of confined phonon modes in [012] SL's and their angular dispersion will be discussed in detail in this paper. Lattice-dynamical calculations are compared with Raman-scattering data; the experimental frequencies of confined and interfacelike modes are close to the predicted values.

The remainder of this paper is organized as follows. A brief presentation of the x-ray characterization of the samples (Sec. II) is followed by a discussion of theoretical results (Sec. III) and a comparison with experimental data (Sec. IV). Section V contains a brief summary and the conclusions.

II. SAMPLE CHARACTERIZATION

The samples studied in this paper are two GaAs/AlAs superlattices (SL's) grown on (012)-oriented, undoped, semi-insulating GaAs substrates by molecular-beam epitaxy (MBE). Details of the growth procedure and the x-ray characterization of the samples have been given in our earlier papers.[1,2] As an illustration of the sample quality, Fig. 1 shows the x-ray-diffraction pattern for the SL samples studied here. These patterns for two [012] GaAs/AlAs superlattices composed of 100 [Fig. 1(a)] and 150 [Fig. 1(b)] SL unit cells are recorded in the vicinity of the asymmetrical (004) GaAs reflection. The diffraction geometry is shown in the inset of Fig. 1(a). The spectra shown in Fig. 1 exhibit a main superlattice peak (0) close to the peak (S) of the GaAs substrate. The angular distance between the SL peak and the substrate peak is related to the Al content. The appearance of sharp, distinct, first-order satellite peaks (+1 and −1) demonstrates the high structural quality of the samples. The slight broadening of the satellite peaks with respect to the main SL peak indicates a small interface roughness (~2 monolayers) at the GaAs/AlAs and AlAs/GaAs transition region.

The satellite-peak broadening is more pronounced for the sample of Fig. 1(b) due to the shorter SL period (40 Å). The x-ray diffraction becomes more sensitive to disorder near the interface with decreasing SL period.[6] In addition, the mean Al content in one SL unit cell in this sample is much lower than in the other sample and consequently the strain is smaller, resulting in weaker

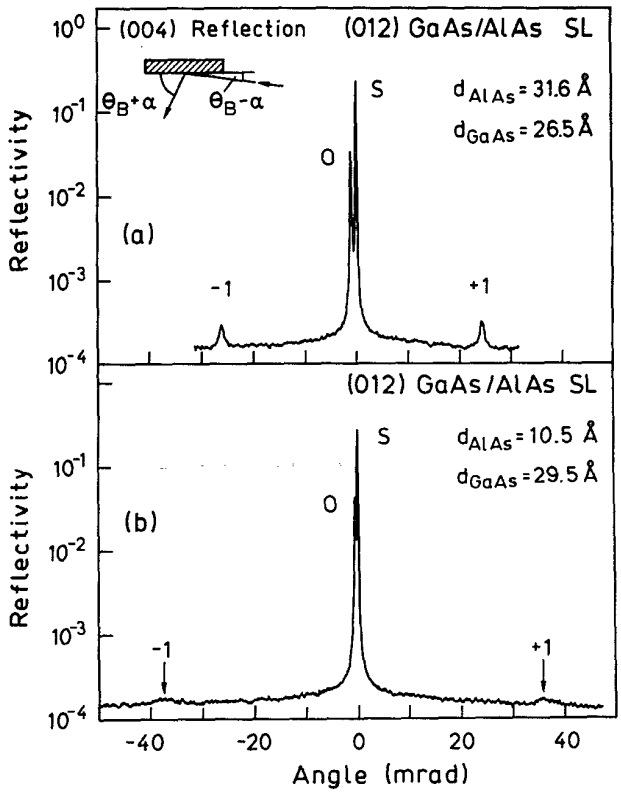

FIG. 1. X-ray-diffraction pattern of the (a) [012] $(GaAs)_{21}/(AlAs)_{25}$ and (b) [012] $(GaAs)_{23}/(AlAs)_8$ superlattices. The inset in (a) represents the geometry of the diffraction arrangement; θ_B is the kinematic (004) Bragg angle and α the angle between the (001) and (012) planes.

satellite-peak intensities. The thicknesses of the individual GaAs and AlAs layers which were obtained by simulation of the experimental diffraction curves using dynamical diffraction theory are also given in Fig. 1. The monolayer spacing along the [012] direction is $d = 1.263$ Å. Consequently, the numbers n_1 of GaAs and n_2 of AlAs monolayers of both constituents of the two samples studied here are (n_1,n_2)=(21,25) and (n_1,n_2)=(23,8), respectively.

III. LATTICE DYNAMICS

A. The model

Lattice-dynamical calculations for GaAs/AlAs superlattices grown along the [012] axis, the results of which have been partially presented previously,[2] were performed using the shell model with parameters fitted to recent neutron data for GaAs.[7] The mass approximation was used for the AlAs layers (all lattice dynamical parameters are the same as for GaAs except for the mass). The interface roughness of the samples was ignored. In the following we first discuss the optical confined modes with wave vectors $\mathbf{q} \parallel [012]$. Then we consider modes with wave vectors perpendicular to the superlattice axis, including interface modes and their angular dispersion. In this paper we focus on the GaAs optical-frequency region; a discussion of the AlAs-like modes would lead to analogous results. We will denote a wave vector in the bulk material by $\mathbf{k}$ and that in the superlattice by $\mathbf{q}$, and the [012], [021], and [100] directions by z', y', and x.

B. Polarization mixing

It was shown in previous papers[1,2] that in the bulk zinc-blende structure phonons with wave vector $\mathbf{k}$ parallel to the [012] direction have mixed longitudinal and transverse polarization (except at the Γ point) due to the low-symmetry group of the $\mathbf{k}$ vector. For the same reason this also applies to superlattice modes, even for those at the zone center. In the bulk materials for small $\mathbf{k} \parallel [012]$ the dominant eigenvector components of the modes of the three optical branches are parallel to [012] for the upper (LO), parallel to $[0\bar{2}1]$ for the middle ($TO_{y'}$), and parallel to [100] for the lowest (TO_x) optical branch. This is indicated in Fig. 2. We use this notation to refer to these branches although the dominant character changes

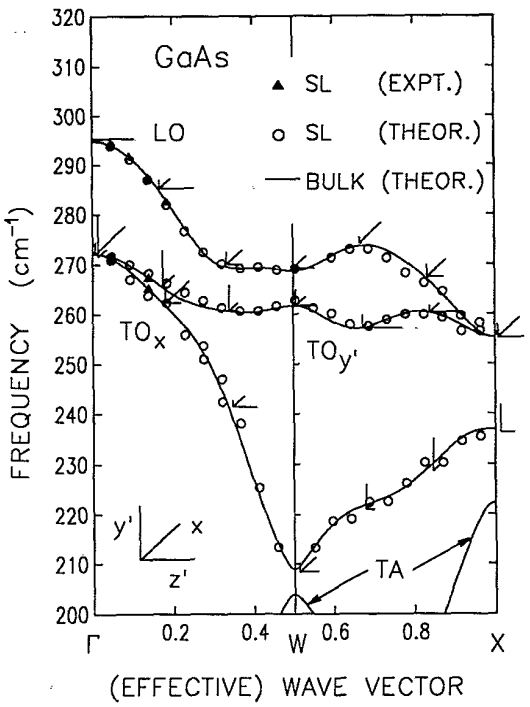

FIG. 2. Experimental (solid triangles) and calculated (open circles) confined-mode frequencies of the $(GaAs)_{21}/(AlAs)_{25}$ superlattice as a function of confinement wave vector q_m, Eq. (1), together with theoretical optical-phonon-dispersion curves of bulk GaAs in the Γ–W–X direction. The plotted bars represent the magnitude of the relative displacement $m_a\mathbf{u}_a - m_c\mathbf{u}_c$ in the three directions [012], $[0\bar{2}1]$, [100], where $\mathbf{u}_k$ and m_k are the displacement and masses of the anion ($k = a$) and cation ($k = c$) in the bulk unit cell, respectively.

with the magnitude of the wave vector along the [012] direction. In the SL this assignment of the main polarization remains valid for confined modes corresponding to these bulk branches (at least for small effective wave vectors q_m, see below). Therefore, we use the notations LO, TO_x, and $TO_{y'}$ also to refer to these SL modes.

The symmetry of the [012] superlattice is monoclinic (point group C_2, space group Pc). The point group consists only of the identity and a twofold rotation around the [100] axis, and therefore there are two irreducible representations. Neglecting polariton effects, the symmetry of the dynamical matrix is broken by the macroscopic electric field even in the limit of the vanishing wave vector. There are only two cases in which the dynamical matrix exhibits the full point-group symmetry for $|\mathbf{q}| \to 0$: the first case is given by $\mathbf{q} \parallel [100]$ and the second by $\mathbf{q} \perp [100]$. In the latter case the rotation around the [100] axis turns $\mathbf{q}$ to $-\mathbf{q}$ which leaves the irregular part of the dynamical matrix invariant as the charge lattice is transformed into itself. Consequently, the confined phonons ($\mathbf{q} \parallel [012]$) are of either A or B symmetry.[8] Displacements of modes with A symmetry are even with respect to the twofold rotation around the [100] axis, while those of the B-symmetry modes are odd. Modes of the [012] superlattice have mixed longitudinal and transverse character. The A modes have a sinelike envelope function, i.e., a node at the center of the layer, for the eigenvector components parallel to [012] and $[0\bar{2}1]$, and a cosinelike envelope function, i.e. an extremum at the center of the layer, for the component parallel to [100]. B modes have cosinelike eigenvector components parallel to [012] and $[0\bar{2}1]$ and a sinelike component parallel to [100].

There is also branch and wave-vector mixing of the lower-frequency optical modes to be discussed in the next section. Neglecting these effects, the eigenvector components have cosinelike or sinelike envelope functions, see Eq. (4) below. From this functional dependence one can deduce an effective (localization) wave vector q_m for each mode, which is defined as in the case of [001] or [011] SL's,

$$q_m = m\pi/d_i, \qquad m = 1, 2, \ldots, \tag{1}$$

where $d_i = a(n_i + \gamma)$ is an effective thickness of the appropriate SL layer (i); n_i is the number of GaAs or AlAs monolayers, respectively, and $a = a_0/2\sqrt{5}$ is the spacing of adjacent monolayers along the [012] direction, with the bulk lattice constant a_0. The value γ describes the extent to which the modes confined to one (GaAs) layer penetrate into the other (AlAs). In the case of the [012] SL's we have found the parameter $\gamma = 0.8$ from our model description. (A value of $\gamma = 1$ for [001] SL's and $\gamma = 0.5$ for [111] SL's gives a good description of the bulk dispersion.[4]) The simple sine and cosine functions are damped near the interfaces due to the fact that these (GaAs-like) modes cannot propagate in the adjacent (AlAs) layers.

As in other growth directions the weighted displacements[9]

$$\mathbf{u}^{(j)}(\mathbf{R}_\kappa) = (-1)^\kappa M_\kappa \mathbf{u}(\kappa|\mathbf{q}, j) \tag{2}$$

with

$$(-1)^\kappa = \begin{cases} +1 & \text{for Ga and Al atoms,} \\ -1 & \text{for As atoms,} \end{cases} \tag{3}$$

turn out to be also useful for the [012] SL. Here j is the branch index and $\mathbf{u}(\kappa|\mathbf{q}j)$ the displacement of the atom κ with mass M_κ at the position $\mathbf{R}_\kappa$. For the envelope functions we replace the discrete positions $\mathbf{R}_\kappa$ by the continuous variable z' along the superlattice axis. The effective wave vector should be common to the functional dependence of the envelope functions of all eigenvector components. Regarding the symmetry restrictions the envelope functions of LO and $TO_{y'}$ eigenvector components have the same functional dependence along the SL axis, different from that of the TO_x components. Thus in the case of confined modes corresponding to the LO and $TO_{y'}$ bulk branches, with dominant eigenvector components parallel to z' and y', respectively, we can approximate the envelope function for B-symmetry modes (m odd) by

$$u_\alpha(z') \sim \begin{cases} \cos[q_m(z' - n_i a/2)] & \alpha = z', y'; \\ \sin[q_m(z' - n_i a/2)] & \alpha = x. \end{cases} \tag{4}$$

For A-symmetry modes (m even) the sine and cosine dependence is reversed. Note that the envelope functions for the TO_x component in the form given above do not have nodes at the interfaces and, therefore, this component has to be damped there.

In the case of confined modes corresponding to the third bulk branch, dominated by the TO_x component, the envelope functions for B-symmetry modes have the same form as given in Eq. (4), but now with m even. For A-symmetry modes (m odd) the sine and cosine dependence is again reversed. For these modes now the LO and $TO_{y'}$ components are damped near the interfaces.

C. Band and wave-vector mixing

Two other features, not appearing in [001] or [111] superlattices, have to be considered (see Fig. 2). The three optical bulk branches have partially overlapping frequency regions. In addition, each branch has a multivalued $\omega(\mathbf{k})$ frequency relation for wave vectors $\mathbf{k}$ parallel to the [012] direction. Since all branches have the same symmetry, a confined mode of a given frequency is generally a superposition of modes corresponding to different bulk branches and/or different bulk wave vectors. (Note that this is less common for SL's grown along higher-symmetry directions.) Thus the discussion of the preceding subsection applies only to confined modes corresponding to the upper part of the bulk LO branch (294–273 cm^{-1}). In this frequency region no other bulk branches exist.

Figure 3 shows envelope functions of the weighted displacement components, Eq. (2), in one SL unit cell for some of the confined GaAs-like modes of the [012] $(GaAs)_{21}/(AlAs)_{25}$ SL with a small $\mathbf{q}$ along the [012] axis. The first column of this figure shows eigenvectors of LO_m modes with $m = 1, 2, 3$, corresponding to the

upper GaAs optical branch and with a main polarization parallel to the SL axis. The second column of Fig. 3 contains the $TO_{y',1}$ and $TO_{y',2}$ modes (corresponding to the $TO_{y'}$ bulk branch). The eigenvectors of these modes are well described by envelope functions given in Eq. (4). (The $TO_{y',1}$ mode contains a small admixture of the LO_{17} vibration.)

However, as shown in the third column of Fig. 3 for the case of the $TO_{x,m}$ modes the mixing with bulk states of other branches cannot be neglected, even for $m = 1$ or $m = 2$. The $TO_{x,2}$ mode, as it would be expected from the idealized discussion above, is mixed with the $TO_{y',3}$ mode. Both states have B symmetry and, *without* mixing, nearly the same frequency. *With* mixing they form a pair of confined modes with one state shifted to somewhat smaller (267 cm^{-1}) and one to somewhat higher (268.2 cm^{-1}) frequency. The same applies to the $TO_{x,3}$ and $TO_{y',4}$ modes (fourth column of Fig. 3) and to further pairs or triplets of modes of the TO_x and $TO_{y'}$ branches but also to modes of the LO branch in the lower frequency region. An example of a mode with a mixed effective wave vector corresponding to the $TO_{y'}$ branch is shown in Fig. 3(l). This mode is a superposition of bulk state with $m = 6$ and $m = 10$.

Figure 2 shows the frequencies of the confined modes (open circles) mapped onto the bulk Brillouin zone along the [012] direction using the corresponding effective wave

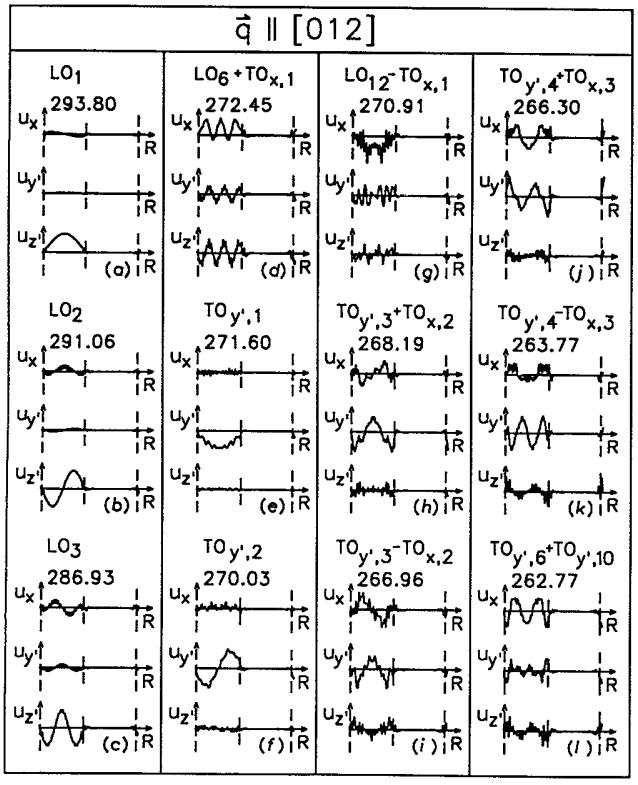

FIG. 3. Envelope functions of the weighted-displacement components $u_\alpha(R)$, Eq. (2), for a number of GaAs-like confined modes of the $(GaAs)_{21}/(AlAs)_{25}$ superlattice, $\mathbf{q} \parallel [012]$.

vectors, Eq. (1), and neglecting superposition. The same effective thickness was used for all modes. Because of the superposition of eigenvectors for many of the confined modes the mapping procedure is not unique in all cases. Most of the confined modes map well onto the bulk branches. The deviations in the upper part of the $TO_{y'}$ and TO_x branches can be explained by the frequency splitting as discussed in the previous paragraph. The confined modes should be bulklike states and thus should map onto the bulk dispersion. Therefore the frequency splitting means that one has to use noninteger values of m for the effective wave vector in these cases instead of an integer m as for modes without mixing.

In the lower part of the TO_x branch in the Γ-W portion (260–210 cm^{-1}), there are two pairs of modes each with the same effective wave vector. In this frequency region the TO_x bulk branch exchanges character with the LO branch. Thus two modes can exist with the same effective wave vector, the frequency being determined by the TO_x component (smaller frequency) or by the LO component (higher frequency). The three lowest-frequency modes lying on this part of the branch have LO character. Beyond the W point this branch regains transverse character by an exchange with a lower-lying mainly transverse polarized acoustic branch, denoted as TA in Fig. 2. Due to their different characters, the two modes to the left and right of the W point have different symmetries, although both are characterized by an even value of m. At the W point there is one mode with optical character missing. Similar results for the LO branch in the W–X region are obtained. There is a character change from LO to TO_x, and again one mode is missing. However, due to multiple superpositon the procedure of assigning effective wave vectors to the modes corresponding to this part of the LO bulk branch is more questionable than for the other parts of the bulk dispersion.

D. Angular dispersion

We now turn to the modes obtained for wave vectors perpendicular to the superlattice axis. In addition to the bulklike confined modes interfacelike modes appear, and, in some cases, they mix with the former. As the $[0\bar{2}1]$ and [100] directions are not equivalent by symmetry, dispersion curves and eigenvectors of the corresponding modes differ for wave vectors parallel to these two directions.

Figure 4 displays the envelope functions of the eigenvector components for several modes with a small $\mathbf{q}$ parallel to the layer plane. The left panel shows modes with $\mathbf{q} \parallel [0\bar{2}1]$, the right one those with $\mathbf{q} \parallel [100]$. In the first case the $TO_{y'}$ eigenvector component is parallel to the wave vector, in the second the TO_x component. Eigenvector components and frequencies differ for the modes shown in the figure. The directional dependence of these frequencies is displayed by the angular dispersion at the Γ point, Figs. 5(a) and 5(b). Figure 5(a) shows the results if the wave vector is rotated in the (100) plane and Fig. 5(b) correspondingly for the $(0\bar{2}1)$ plane (starting with $\mathbf{q} \parallel [012]$, i.e., $\theta = 0$).

Only infrared-active modes can show angular dispersion. Such dispersion arises from the fact that their macroscopic electric field depends on the wave-vector direction. The A- and B-symmetry optical modes of the [012] SL are all infrared active, but the most dramatic angular dispersion appears in the frequency range between the bulk LO and TO Γ-point frequencies. The frequency of the infrared-active modes depends upon the direction of the wave vector and the larger the longitudinal component of the electric dipole moment the higher the frequency. The eigenvectors of the modes with $\mathbf{q} \perp [012]$ partially display a superposition (mixing) of confined bulklike modes with the interface modes (IF). In the electrostatic continuum model[10] one does not obtain this superposition; this is due to the neglect of dispersion of the bulk optical branches.[11] We refer to these superposed modes as interfacelike modes.[12] We distinguish between IF_x, $IF_{y'}$, and $IF_{z'}$ interface modes according to their contribution to either the x, y', z' components of the eigenvectors.

As in the continuum model interface modes at GaAs optical frequencies for $\mathbf{q} \perp [012]$ and $|\mathbf{q}| \approx 0$ have nearly constant eigenvectors within the GaAs layer but decay, close to the layer boundary, to a small, but nonzero value. The atoms of the AlAs layer vibrate with this same small amplitude. The middle curve of Fig. 4(e) and the upper one of Fig. 4(k) display this nearly flat behavior in the GaAs layer. The lower curves in Figs. 4(b) and 4(c) exemplify the mixture of interfacelike (flat) and confined (oscillatory) modes.

From the analysis of the angular dispersion curves of Figs. 5(a) and 5(b) we draw the following conclusions.

Only LO_m, $TO_{y',m}$, and $TO_{x,m}$ modes of small in-

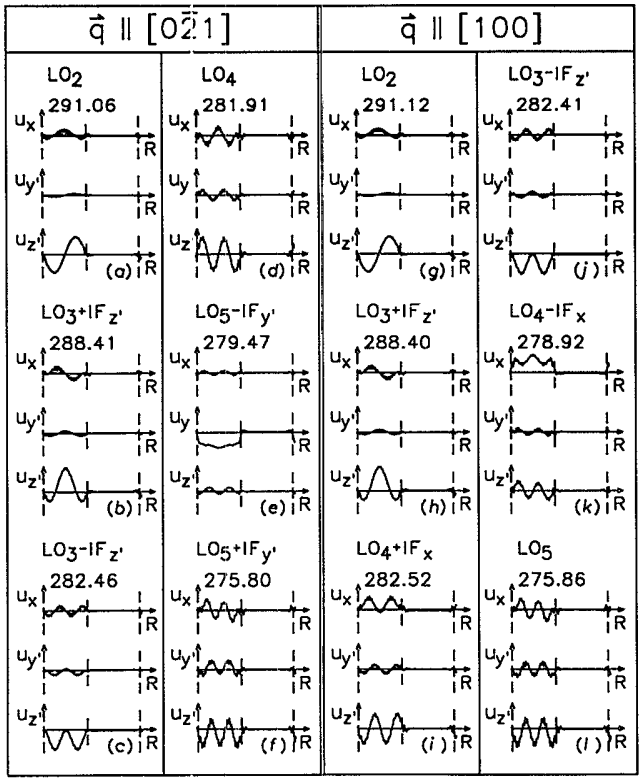

FIG. 4. Envelope functions as in Fig. 3 for a number of GaAs-like zone-center optical modes of the $(GaAs)_{21}/(AlAs)_{25}$ superlattice for $\mathbf{q}$ perpendicular to the layer axis and $|\mathbf{q}| \to 0$. Left panel $\mathbf{q} \parallel [0\bar{2}1]$; right panel $\mathbf{q} \parallel [100]$.

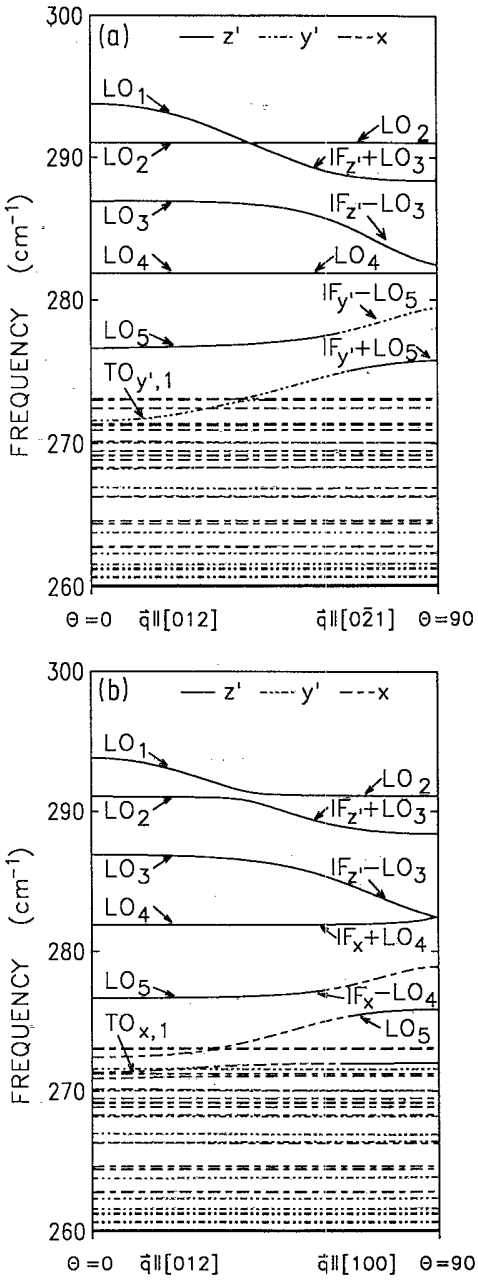

FIG. 5. Calculated angular dispersion of the optical modes of the $(GaAs)_{21}/(AlAs)_{25}$ superlattice for infinitesimal $|\mathbf{q}|$. (a) $\mathbf{q}$ varies in the (100) plane; (b) $\mathbf{q}$ varies in the $(0\bar{2}1)$ plane. The solid, dashed, and dash-dotted lines represent modes predominantly polarized along z' (LO), x (TO_x), and y' ($TO_{y'}$), respectively.

dex m ($m = 1$ or $m = 3$) contribute significantly to the infrared activity: for higher index m there is nearly complete compensation of the dipole moments of lobes with opposite signs. Therefore the former modes suffer the most drastic electrostatic-field effects.

Below 273 cm^{-1}, the zone-center TO frequency of bulk GaAs, the confined modes, show only small (273–270 cm^{-1}) or vanishing (below 270 cm^{-1}) angular dispersion. The eigenvectors remain the same as for $\mathbf{q} \parallel [012]$. An example of an eigenvector of such a mode exhibiting no interface character is displayed in Fig. 4(d).

Since A-symmetry modes have an electric dipole moment parallel to the [100] direction, they show no angular dispersion for $\mathbf{q}$ varying in the (100) plane. As stated in Sec. III B for wave vectors parallel to this plane in the limit $|\mathbf{q}| \to 0$ the unretarded dynamical matrix has full point-group symmetry, and therefore the classification in terms of A- and B-symmetry modes remains valid. Thus the crossing of the dispersion branches of A- and B-symmetry modes is allowed, as shown in Fig. 5(a).

As both A- and B-symmetry modes for $\mathbf{q} \parallel [012]$ and $|\mathbf{q}| \to 0$ have a dipole moment parallel to the $(0\bar{2}1)$ plane, their frequencies depend on the angle θ between the wave vector parallel to the $(0\bar{2}1)$ plane and the [012] axis. For $\mathbf{q}$ in the $(0\bar{2}1)$ plane, the symmetry of the dynamical matrix is lowered due to the macroscopic electric field. The symmetry group consists only of the identity and therefore even in the limit $|\mathbf{q}| \to 0$ anticrossings occur in the dispersion branches of these modes, as shown in Fig. 5(b).

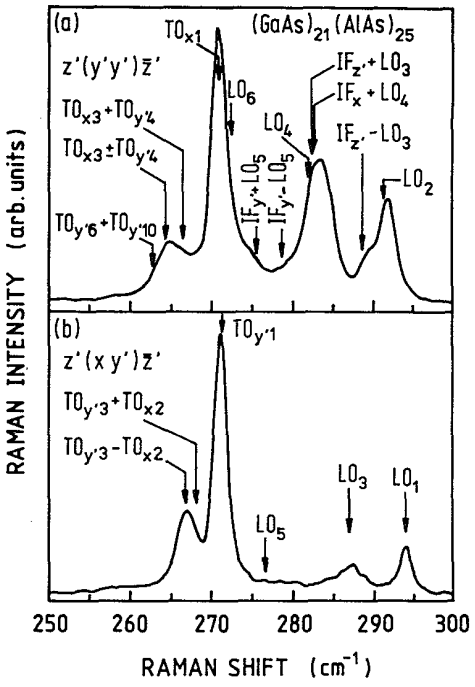

FIG. 6. (a) Polarized and (b) depolarized Raman spectra of the [012] $(GaAs)_{21}/(AlAs)_{25}$ superlattice at 80 K in backscattering configuration ($x \parallel [100]$, $y' \parallel [0\bar{2}1]$, $z' \parallel [012]$). The calculated frequencies of the confined and interfacelike modes are indicated by arrows.

IV. EXPERIMENT

The Raman spectra were measured in backscattering geometry using a Spex Industries double monochromator (Model 1403) with a conventional photon counting detection system. The excitation source was the 5145 Å line of an Ar^+-ion laser. Measurements were made at liquid-nitrogen temperature.

Raman spectra of the (21,25) and (23,8) superlattices in the GaAs optical-phonon spectral region are given in Figs. 6 and 7. In Fig. 8 we show the Raman spectra of the same samples in the AlAs optical-phonon region. The frequency of the exciting laser line is away from all possible resonances.

From the symmetry properties of the eigenvectors it follows that the polarized spectra are caused by modes of A symmetry, while the depolarized ones are caused by modes of B symmetry. The Raman tensors and selection rules are given in Table I of Ref. 2.

In the GaAs optical-phonon frequency region (Figs. 6 and 7) a rather good agreement of experimental assignment with calculated phonon frequencies is found. Four confined modes of A symmetry are observed in the polarized spectra, Figs. 6(a) and 7(a), and of B symmetry in the depolarized spectra, Figs. 6(b) and 7(b), with dominantly longitudinal (LO_m) and transverse ($TO_{y',m}$ and $TO_{x,m}$) polarization, respectively. Since several modes

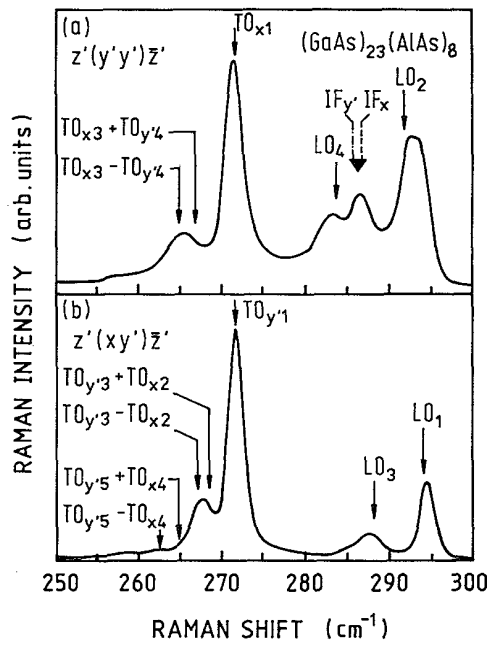

FIG. 7. (a) Polarized and (b) depolarized Raman spectra of the [012] $(GaAs)_{23}/(AlAs)_8$ superlattice at 80 K. Symbols as in Fig. 6.

which are superpositions with the expected $TO_{x,1}$ mode exist around 270 cm^{-1}, the peak marked as $TO_{x,1}$ in Figs. 6(a) and 7(a) is probably a superposition of all these modes. This would explain the larger width of this peak as compared with the $TO_{y',1}$ peak. The same can be stated for the $TO_{x,3}$ peak, where a superposition with the $TO_{y',4}$ mode is possible. The $TO_{y',6}+TO_{y',10}$ mode, see Fig. 3(l), with a strong TO_x component may give scattering around 263 cm^{-1}.

In addition to the confined modes, structures which we assign to interfacelike modes are observed in Figs. 6 and 7: The shoulder in Fig. 6(a) at 289 cm^{-1} is attributed to the $IF_{z'}$-LO_3 mode, whose eigenvector components are shown in Fig. 4(b). The increase in intensity and broadening of the LO_4 confined mode is due to its superposition with the LO_4+IF_x and $LO_3+IF_{z'}$ interfacelike modes with eigenvector components shown in Figs. 4(c) and 4(i), respectively.

The calculated frequencies and the experimental Raman spectra of the confined and interfacelike modes of the (23,8) SL, see Figs. 7(a) and 7(b), are also in good agreement. Compared with the (21,25) SL the GaAs-like confined modes are shifted to somewhat higher frequencies due to the larger GaAs layer thickness and correspondingly smaller effective wave vector. Due to the much smaller AlAs layer thickness the interfacelike modes

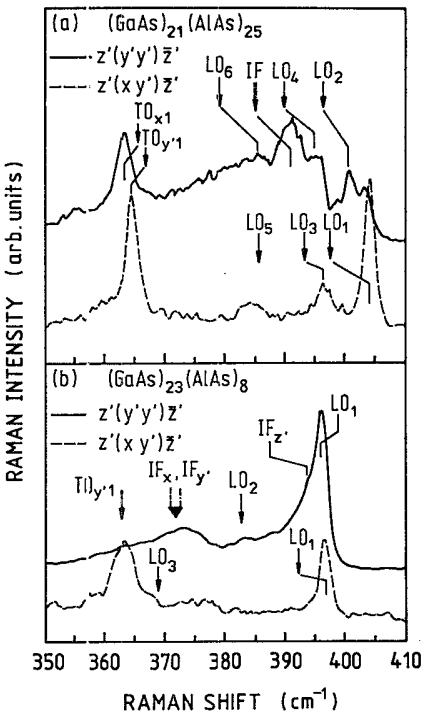

FIG. 8. Raman spectra of the (a) [012] $(GaAs)_{21}/(AlAs)_{25}$ and (b) [012] $(GaAs)_{23}/(AlAs)_8$ superlattices at 80 K in the optical-phonon region of AlAs. Indicated by arrows are the calculated superlattice-mode frequencies which in our simple model of AlAs turn out to be too small. The assignments of the Raman peaks are shown by lines.

IF_x and $IF_{y'}$ are shifted to higher and the $IF_{z'}$ to lower frequencies. We note that the eigenvector components of the interfacelike modes denoted $IF_{y'}$ and IF_x in Fig. 7(a) are very similar to those of the LO_5–$IF_{y'}$ and $LO_4\pm IF_x$ modes of the (21,25) superlattice in Figs. 4(e), 4(i), and 4(k), respectively. The $IF_{z'}$ mode is superposed with the LO_5 instead of the LO_3 bulklike confined mode.

Figure 8(a) shows spectra of AlAs-like confined LO_m modes with indices up to $m = 5$ for the (21,25) sample. The mapping onto the bulk dispersion of these five frequencies indicates that there is much more dispersion in the AlAs bulk material along [012] than along the more commonly studied [001] direction. In the mass approximation the AlAs bulk phonon frequencies are not exactly reproduced: along a cubic axis the whole LO branch is too low by about 6 cm^{-1} and the TO branches too high by about 4 cm^{-1} in comparison with a recent *ab initio* calculation of the AlAs dispersion.[13] If we shift our theoretical bulk dispersion curves along the [012] wave-vector direction (and also the confined mode frequencies) to coincide with experimental data at the Γ point, the experimentally obtained frequencies of the AlAs-like confined modes indicate that the dispersion of the LO branch in our model is underestimated.

Only one transverse confined mode of each kind, $TO_{y',1}$ and $TO_{x,1}$, is resolved for this sample. It is interesting to note that a frequency shift between the $TO_{x,1}$ and $TO_{y',1}$ modes is experimentally observed, see Fig. 8(a). This splitting is related to the nondegeneracy of the TO_x and $TO_{y'}$ bulk optical branches along the [012] direction. (For the GaAs-like peaks this splitting is not resolved.) As in the GaAs frequency region the broad $TO_{x,1}$ peak indicates that possibly further confined modes contribute to this peak.

The Raman spectra of the AlAs optical-frequency region for the (23,8) sample are given in Fig. 8(b). Only the LO_1 and $TO_{y',1}$ peaks are clearly observed. The lack of well-resolved peaks originating from other confined modes may be due to the interface roughness of two monolayers compared to the layer thickness of only eight monolayers. For this sample our model gives an interfacelike $IF_{z'}$ mode with a somewhat smaller frequency than that of the LO_1 mode. This fact and the interface roughness may explain the appearance of the broad peak at the LO_1 frequency in the polarized spectrum, Fig. 8(b). IF_x and $IF_{y'}$ modes are found close to the frequencies of the transverse modes. The different frequencies of the interfacelike modes of the (21,25) and the (23,8) sample are due to the different ratio of the layer thicknesses in qualitative agreement with the electrostatic continuum model.[14]

V. SUMMARY

We have performed a shell-model calculation of the phonon frequencies and eigenvectors of [012] GaAs/AlAs superlattices. The zone-center optical modes display angular dispersion. The calculated frequencies of the con-

fined and interfacelike modes show very good agreement with measured TO and LO confined and IF mode frequencies in the GaAs optical-phonon region.

Under ideal conditions (perfect interfaces, infinitely large number of layers, bulk-crystal Raman tensors) one would expect the interface modes to be Raman inactive. Deviations from the backscattering geometry would activate these modes. With nonideal interfaces it seems hopeless to calculate the scattering intensities, for the most ideal case, to unravel the deformation-potential and Fröhlich contributions.[15,16]

The assignment of effective wave vectors q_m to confined modes in the [012] superlattice has been found to be much more complicated than in either of the [001], [111], or [110] cases. On the one hand this complication is due to the mixed longitudinal and transverse character of superlattice modes, on the other hand the confined modes can be superpositions of bulklike modes corresponding to different bulk branches, and therefore with different effective wave vectors, since the three optical bulk branches have overlapping frequency regions. Our investigations indicate that the proper assignment of q_m can only be made by comparison with theoretical eigenvector envelope functions. One has to keep in mind, however, that different models may give somewhat different results.

ACKNOWLEDGMENTS

The technical assistance of A. Fischer with MBE growth and H. Hirt, M. Siemers, and P. Wurster with Raman measurements is gratefully acknowledged. Part of this work was sponsored by the Bundesministerium für Forschung und Technologie of the Federal Republic of Germany and the Deutsche Forschungsgemeinschaft. Z.V.P. gratefully acknowledges financial support from the Alexander von Humboldt Foundation.

*Permanent address: Institute of Physics, P.O. Box 57, 11000 Belgrade, Yugoslavia.

[1] Z. V. Popović, M. Cardona, L. Tapfer, K. Ploog, E. Richter, and D. Strauch, Appl. Phys. Lett. **54**, 846 (1989).

[2] Z. V. Popović, M. Cardona, E. Richter, D. Strauch, L. Tapfer, and K. Ploog, Phys. Rev. B **40**, 1202 (1989); **40**, 1207 (1989).

[3] Z. V. Popović, M. Cardona, E. Richter, D. Strauch, L. Tapfer, and K. Ploog, Phys. Rev. B **40**, 3040 (1989).

[4] Z. V. Popović, H. J. Trodahl, M. Cardona, E. Richter, D. Strauch, and K. Ploog, Phys. Rev. B **41**, 5904 (1990).

[5] B. Jusserand and M. Cardona, in *Light Scattering of Solids V*, edited by M. Cardona and G. Güntherodt (Springer-Verlag, Heidelberg, 1989), p. 49.

[6] L. Tapfer, N. Kobayashi, T. Makimoto, and Y. Horikoshi, J. Phys. **48**, C5-521 (1987).

[7] D. Strauch and B. Dorner, J. Phys. Condens. Matter **2**, 1457 (1990).

[8] The classification of the confined modes according to A and B symmetry is strictly valid only for $|\mathbf{q}| = 0$, since the twofold rotation axis parallel to [100] is perpendicular to the direction of the wave vectors corresponding to the confined modes. However, the confinement, resulting in dispersionless branches, leaves the shape of the displacements in the superlattice unit cell unchanged.

[9] E. Richter and D. Strauch, Solid State Commun. **64**, 867 (1987).

[10] R.E. Camley and D.L. Mills, Phys. Rev. B **29**, 1685 (1984).

[11] F. Bechstedt and H. Gerecke, Phys. Status Solidi B **156**, 151 (1989). A critical comparison of the continuum approach and microscopic model was also recently given by K. Huang and B. Zhu, Phys. Rev. B **38**, 13 377 (1989).

[12] At $|\mathbf{q}| = 0$ the eigenvectors form a complete set, and the eigenvectors corresponding to $\mathbf{q} \perp [012]$ can be expressed as linear combinations of those corresponding to $\mathbf{q} \parallel [012]$. Therefore, the interface modes can be regarded as a superposition of confined modes rather than an extension of the eigenvector space. However, whereas most of the amplitudes of the LO_1, $TO_{x,1}$, and $TO_{y',1}$ confined modes turn into those of the interfacelike modes as the wavevector is rotated away from the SL axis, the confined modes with higher index m remain nearly unchanged or gain an admixture of interfacelike character.

[13] S. Baroni, P. Giannozzi, and E. Molinari, Phys. Rev. B **41**, 3870 (1990). Calculating the AlAs dispersion in the mass approximation using GaAs *ab initio* force constants the authors find a quasirigid shift of the LO branch along a cubic axis to lower frequencies by about 4 cm^{-1} compared with the results of a full self-consistent calculation.

[14] A.K. Sood, J. Menéndez, M. Cardona, and K. Ploog, Phys. Rev. Lett. **54**, 2115 (1985).

[15] Bang-fen Zhu, Kun Huang, and Hui Tang, Phys. Rev. B **40**, 6299 (1989); Kun Huang, Bang-fen Zhu, and Hui Tang, *ibid.* **41**, 5825 (1990).

[16] F. Hersel, D. Suisky, J. Röseler, and R. Enderlein (unpublished).